The structure degradation of a silty loess induced by long-term water seepage

Lu Zuo[a], Ling Xu[a,#], Beatrice Anne Baudet[b], Chongyang Gao[a], Chuang Huang[a]

[a]Department of Civil Engineering, School of Human Settlements and Civil Engineering, Xi'an Jiaotong University, Xi'an, China

[b]Department of Civil, Environmental and Geomatic Engineering, University College London, U.K.

[#]corresponding author

Abstract

Loess is a typical silt-sized Aeolian soil that is widely deposited and possesses a fragile soil structure susceptible to collapse upon wetting. The instability of shallow loess slopes is well documented, but deeper failures triggered by rainfall and irrigation can also occur. In the case of long-term seepage, clay particles and salts have been observed to leach out of the loess slopes. This paper presents a systematic laboratory study of the effects of water conditions on the mechanical behaviour of silty loess, with isotropic compression and bender element tests carried out on natural and reconstituted loess recovered at 10m depth from a site in China. The results show that saturation causes reduction in both the compression yield stress and small strain stiffness of the soil, and that after being exposed to seepage, they decrease further. The possible mechanism of structure degradation is investigated by means of microscopic and chemical analyses, and it is found that seepage will cause the pore ions concentration to reduce with a loss of clay mineral bonding strength, resulting in the detachment of silt particles from aggregates. This work highlights the importance of monitoring the water outflow in the field at the loess slope edge, since it may causes large deformation in the long-term.

Keywords

Loess, Laboratory tests, Seepage, Soil structure, Compression, Small strain stiffness

Introduction

Loess is a typical silt-sized Aeolian soil that is encountered all around the world (Li et al., 2016), with wide deposits in northwest China (Heller & Liu, 1982). Loess has long been studied because of its collapsible mechanical properties. It is commonly reported that loess suffers a great loss of strength when subjected to wetting, for example after rainfall or irrigation, (Derbyshire et al., 1994; Muñoz-Castelblanco et al., 2011; Jiang et al., 2012; Zhang et al., 2017), and this property is believed to be the main reason for the frequently occurring collapse of shallow loess slopes (Zhang et al., 2009; Xu et al., 2011; Xu et al., 2014; Leng et al., 2018). Deeper failures have also been observed, sometimes in the form of landslides, but they are less understood. These failures initiate underneath the water table, where the loess is saturated (Tu et al., 2009, Zhang et al., 2009; Xu et al., 2012; Tang et al., 2015; Zeng et al., 2016), so that the mechanism behind the strength loss cannot be attributed to the changes in soil micro-structure or in effective stress state variables commonly associated with shallow slopes (Li et al., 2016). For the saturated loess soil beneath the water table, factors affecting the stability can be a rise in the ground water table that will enhance the outflow in the field at the slope edges or along the valleys during a long period (Xu et al., 2011; Zhang et al., 2013; Li et al., 2014). Salt, which is reported widely to exist in loess soil (Zhang et al., 2013; Li et al., 2016), will then leach out as shown in figure 1. This will mainly affect the soil structure and may potentially have an impact on the soil strength further. In former studies on loess under water seepage condition, the hydraulic characteristics, such as hydraulic conductivity, have generally been the focus instead of the mechanical properties (e.g. Zhao et al., 2016; Wang et al., 2018). On the other hand, published experimental works on the mechanical behaviour of loess are for either unsaturated or for simply saturated (short-term soil-water interaction) conditions (e.g. Zhou et al., 2014; Zhang & Wang, 2018; Xie et al., 2018; Liu et al., 2019), while the mechanical properties of loess undergoing water seepage (long-term soil-water interaction) have not been studied in controlled conditions.

Figure 1 The leaching out of salt induced by water seepage in field

It is well established that the strength of clays is affected by the pore solution concentration. Bjerrum (1954) and Bjerrum & Rosenqvist (1956) found that when subjected to a hydraulic gradient resulting in leaching out of salts, the shear strength of natural marine clays decreases. Clays treated with NaCl solution, when exposed to distilled water, see their residual shear strength decrease; this was observed in bentonite (Di Maio & Fenelli, 1994; Di Maio, 1996; Di Maio & Scaringi, 2016), illitic soils (Di Maio et al., 2015) and mudstone soil from Japan (Tiwari et al., 2005, Tiwari & Ajmera, 2015). When seepage occurs, not only will the pore solution concentration change, but the fine particles may move through the soil matrix by suffusion, resulting in the soil internal instability (Fannin & Slangen, 2014; Hunter & Bowman, 2018). For intact loess, although the soil structure is mainly made up of primary (large-sized) silt particles and silt particle aggregates, the coating and bonding between silty particles, reported to consist of clay or calcium carbonate (Xu & Coop, 2016; Li et al., 2016; Ng et al., 2017a), may detach and erode within the soil, creating instability.

Previous studies on loess' mechanical behaviour focused on the compression and shearing behaviour under a limited range of water conditions and stress levels (Rogers et al., 1994; Wen & Yan, 2013; Jiang et al., 2014, Xu & Coop, 2016, 2017; Ng et al., 2017a; Xu et al., 2018; Liu et al., 2019). Tests on saturated loess have demonstrated how the loess structure dominates its mechanical behaviour (e.g. Xu & Coop, 2016). The small strain behaviour of loess received much less attention (Ng et al., 2017b; Song et al., 2017; Liu et al., 2019). In clays and sand, the relationship between the small strain stiffness, denoted as G_0, and the mean effective stress, p', is well established for states on the normal compression line as:

$$\frac{G_0}{p_r} = A(\frac{p'}{p_r})^n \tag{1}$$

where p_r is a reference stress, A and n are soil parameters (e.g. Viggiani & Atkinson, 1995; Jovičić & Coop, 1997) related to soil structure, such as particle arrangements and contacts (Cascante & Santamarina, 1996; Cho et al., 2006; Lee et al., 2007). For structured soil, such as the loess in this study, studying the mechanical properties at small strains and its characteristic parameters should thus provide useful complementary information on the evolution of structure.

This paper presents results from laboratory tests on undisturbed and reconstituted silty loess subjected to isotropic compression under three different water conditions: at the natural water content (constant-water content test), simply saturated (traditional isotropic compression test after a short saturation stage) and after a long period of seepage. The tests were carried out to stress levels high enough for the soil to reach the normal compression line, and they were complemented by bender element tests. The specimens subjected to long-term seepage prior to compression were further investigated with mercury intrusion porosimetry and scanning electron microscope tests, and a possible mechanism for structure evolution is discussed.

Materials, testing apparatus and procedures

Materials

The soils tested were recovered at a depth of 10m in a typical location of silty loess deposition near Lanzhou city, China. Care was taken that the samples did not experience any previous water infiltration. The structure was kept intact by using block sampling, each block sample trimmed by hand and carefully sealed with layers of cling film and tape. A cutting ring was used to make undisturbed specimens from the blocks, while the rest of the soil was used to make reconstituted specimens and determine the soil properties. The particle size distribution (PSD) of the silty loess was determined by the hydrometer method. Figure 2 shows that more than 85% of the soil is of silt size, with clay content about 5%. The specific gravity is 2.70, and the plastic and liquid limit are 17·8% and 26·4% respectively. The minerals of the silty loess determined by X-ray diffraction (XRD) are summarized in table 1; they consist mainly of quartz, albite, calcite, and the clay mineral illite.

Table 1 Mineral composition of the silty loess

non-clay minerals (%)						clay minerals (%)			
Quartz	Albite	Calcite	Dolomite	Potassium feldspar	Hornblende	Illite	Chlorite	Illite/smectite (I/S)	Kaolinite
37.1	17.4	13.0	4.9	2.2	2.2	12.9	4.5	3.0	2.7

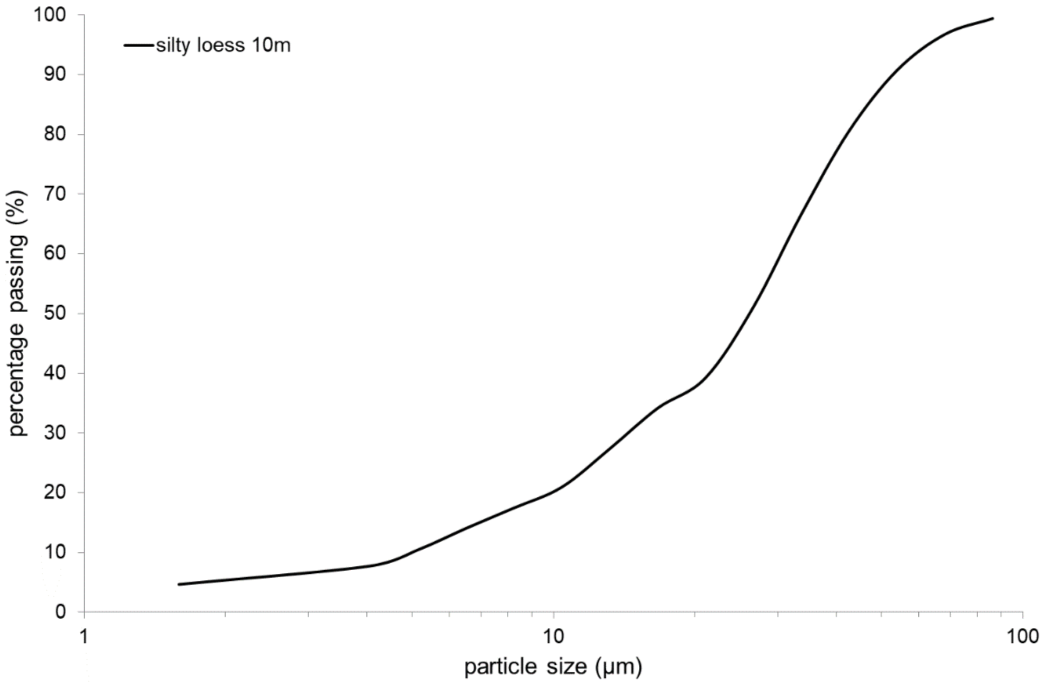

Figure 2 Particle size distribution curve of silty loess

Testing apparatus and procedures

The isotropic compression tests were conducted in a triaxial system equipped with bender elements and local strain measuring LVDTs as illustrated in figure 3. The tested sample size was 50mm in diameter and 100mm in height. A pair of vertical bender elements was embedded in the top cap and pedestal to measure the small strain stiffness during compression (figure 3, part 10). A special oscilloscope was used as signal generator with a maximum applied voltage of 12V, and to receive the signals. The time-domain method, more specifically the first arrival method was used to determine the small strain stiffness. The time delay between transmitter and receiver elements was calibrated by "tip to tip" method. To minimize the uncertainty brought by near-field effects, a series of sinusoidal input signals of frequencies in the range 5-15kHz was used, and a common travel time was obtained by comparing all the received signals. Two LVDTs for local axial strain measurement were directly glued on the specimen membrane (figure 3, part 11-13), and a system recommended by Ackerley et al. (2016) was set up for the local radial strain measurement (figure 3, part 3-7). The measuring range of the LVDTs was 0−10mm and the resolution was ±0.0004mm. Before tests, the triaxial cell, loading frames, and pressure controllers were all confirmed to be working normally, and the transducers, including load cell, water pressure transducer, and LVDTs were all calibrated.

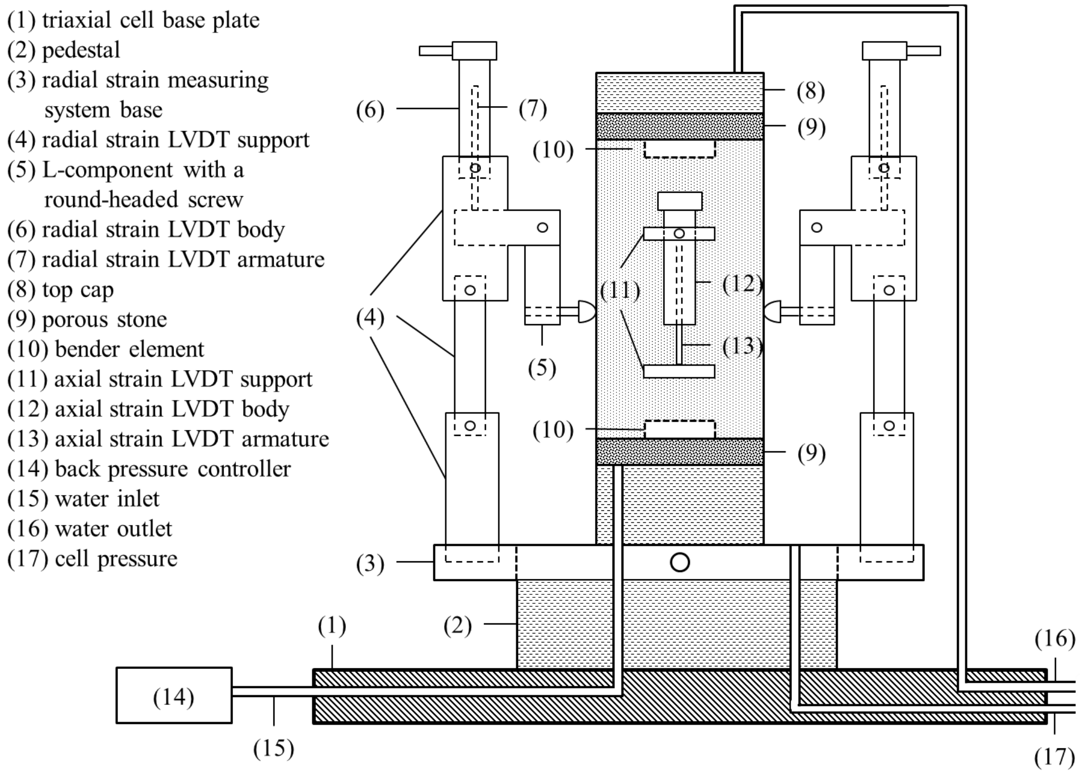

Figure 3 Schematic diagram triaxial apparatus equipped with vertical bender elements and axial and radial LVDTs

Both undisturbed and reconstituted specimens were tested. For undisturbed specimens, a cutting ring with a chosen dimension was placed on the soil block and some downward pressure was applied, then the soil out of the ring edge was cut off by hand carefully to avoid any micro-cracks or structure destruction and the specimen was trimmed into the ring gradually (Xu & Coop, 2016). For reconstituted specimens, the moist tamping method was used for sample preparation. The soil was first oven-dried and grinded to aggregate sizes less than 0.3mm to remove the existence of intact structure as much as possible. Then the soil was weighed according to the designed initial void ratio for the experiments (loose, medium-dense and dense) and mixed well at an initial water content of 3.65%, which is equal to the natural water content of the silty loess, until an homogeneous fabric was obtained. Then the soil was compacted on the pedestal in 4 even layers with the help of a split mould. Each layer had a thickness of 25mm.

After the specimens were set up in the triaxial system, three different initial water conditions were applied before compression: constant-water content condition, simply saturated condition, and after seepage condition. For the constant-water content condition, the specimen was compressed in unsaturated condition, no further de-aired water, flushing or saturation stage was applied ~~to the specimen~~, so the initial water content was kept constant at the natural water content (3.65%), and the water outlet (figure 3, part 16) was connected to the atmosphere during compression. For the simply saturated condition, the specimen was first flushed with CO_2 and then a water head of 1m (9.8kPa pressure) was controlled (figure 3, part 14) to achieve water flushing through the specimen from the water inlet (figure 3, part 15). Water flushing was stopped when there was no air bubble coming out and a water drop could be observed at the water outlet (figure 3, part 16). Then the specimen was subjected to back pressure saturation to achieve a B-value above 0.95 (back pressure value: 300 kPa). For the after-seepage condition, similarly, the specimen was flushed with CO_2 and 1m water head de-aired water in turn, but here to ensure steady-state seepage, the water flushing was not stopped until the coefficient of permeability, k, became stable (the development of k during seepage will be shown in detail later in the test results).

Then a back pressure saturation procedure (back pressure value: 300 kPa) was applied to achieve a B-value above 0.95. After the initial desired water condition was achieved, the cell pressure was increased in steps to conduct an isotropic compression test, to a maximum confining pressure of 1.5MPa.

As a supplement, one-dimensional compression tests were conducted in an oedometer cell on samples of 75.7mm in diameter and 30mm in height. The deadweight was added in steps, to a maximum vertical stress of around 3.1MPa (total vertical stress). A back pressure valve was connected to the bottom of the specimen, and to the atmosphere (back pressure equals to 0kPa) during one-dimensional compression for the saturated specimens. Similarly to the isotropic compression tests, both undisturbed and reconstituted specimens in three different initial water conditions were tested, and for the after-seepage condition, de-aired water of 1m water head was first controlled to flow in from the bottom to the top surface of the specimen until the coefficient of permeability became constant. More detailed information on the compression tests conducted is summarized in table 2.

Table 2 Summary of tests conducted with the silty loess

preparation method	tests conducted	sample diameter (mm)	maximum verticle stress/confining pressure (kPa)	water condition	number of specimens tested	initial void ratio
undisturbed	1-D compression	75.7	3110	constant-water content	2	0.979, 1.030
				simply saturated	2	0.953, 0.967
				after seepage	2	0.975, 0.966
	isotropic compression bender element	50	1500	constant-water content	2	0.983, 0.973
				simply saturated	2	0.980, 0.987
				after seepage	2	0.969, 0.959
			50	constant-water content	1	0.970
				simply saturated	1	0.970
				after seepage	1	0.970
reconstituted	1-D compression	75.7	3110	constant-water content	3	0.975, 0.959, 0.794
				simply saturated	3	0.982, 0.889, 0.804
				after seepage	3	0.919, 0.867, 0.803

	isotropic compression bender element	50	1500	constant-water content	3	1.000, 0.922, 0.859
				simply saturated	3	1.000, 0.948, 0.858
				after seepage	3	1.000, 0.948, 0.857
			50	constant-water content	1	0.986
				simply saturated	1	0.986
				after seepage	1	0.986

Three different methods were used for the calculation of the initial specific volume, v_i, as listed in equations (2)–(4) below, which take account of the degree of saturation of the sample (Rocchi & Coop, 2014).

$$v_i = \frac{G_s \gamma_w}{\gamma_{di}} \tag{2}$$

$$v_i = \frac{G_s \gamma_w (1 + w_i)}{\gamma_i} \tag{3}$$

$$v_i = \frac{G_s \gamma_w (1 + w_f)}{\gamma_f (1 - \varepsilon_v)} \tag{4}$$

where G_s is the specific gravity, γ_w is the unit weight of water, γ_{di} is the initial dry unit weight, γ_i and γ_f are the initial and final bulk unit weights respectively, w_i and w_f are the initial and final water content respectively, and ε_v is the volumetric strain. An average was taken, and calculated void ratios outside a ±0.02 range from the mean value were discarded.

Performance of the local LVDTs

With the measurement of axial and radial local LVDTs, the deformation during saturation, seepage and compression can be determined. This is particularly important for monitoring the volumetric deformation of the specimen with constant-water content conditions during isotropic compression, since it cannot be determined by the change in volume of water. With the assumption that the specimen is homogenous in shape and fabric, the volumetric strain ε_v can be calculated as:

$$\varepsilon_v = \varepsilon_a + 2\varepsilon_r \tag{5}$$

where ε_a is the axial strain, calculated as the average value of the axial strains determined by the two axial local LVDTs, and ε_r is the radial strain, calculated as the average value of the radial strains determined by the two radial local LVDTs.

For the specimens in simply saturated and after seepage conditions, ε_v can be determined by both local LVDTs and back volume, thus, by comparing these two results, an evaluation of the reliability of the local LVDTs measurements can be achieved. The ratios of the volumetric strain increments ($\Delta\varepsilon_v$) determined by the two methods at different loading stages are illustrated in figure 4. It shows that at relatively low stress levels, $\Delta\varepsilon_v$ measured with back volume is always larger than that measured with local LVDTs, especially when the stress is less than 50kPa, and the difference is more significant for the undisturbed specimens. This may be due to the initial local inhomogeneity in specimen shape or fabric, thus the deformation of the local areas cannot fully represent the overall deformation of the whole sample. As the confining pressure increases, the difference reduces quickly and the results show good agreement with each other, indicating that the initial structure becomes less heterogeneous during isotropic loading. The local LVDTs measurements were thus assumed to be reliable at high stress levels, while at low stress levels a correction coefficient was applied, which was possible since the absolute values of $\Delta\varepsilon_v$ are relatively small. The local LVDTs measurements and correction coefficients extracted from figure 4 were used to calculate the volumetric strain of the specimen with constant-water content condition during isotropic compression.

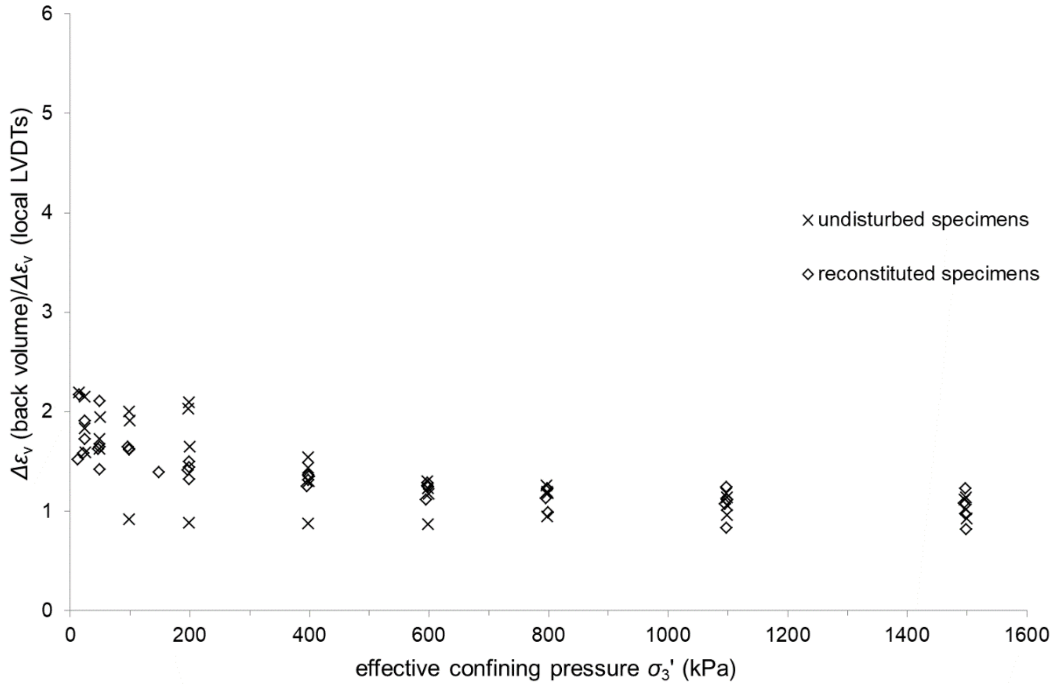

Figure 4 Ratios of the volumetric strain increments determined by two methods at different loading stages

Compression behaviour

The compression curves obtained from the one-dimensional and isotropic compression tests on undisturbed specimens are plotted in figure 5. The data for the two types of saturated specimens (i.e. including those after seepage conditions) are plotted in terms of specific volume, v, against effective stress, σ_3' for the triaxial tests and σ_v' for the oedometer tests. The procedure explained above (eq. (2) to (4)) ensured the accuracy of the location of the normal compression lines (NCLs) (e.g. Xu & Coop, 2017, Li & Coop, 2019). Normal compression lines determined from the data points after yielding were fitted to the data (Fig. 5). It is clear that two distinct, almost parallel NCLs are reached under simply saturated or after-seepage conditions. The NCL after seepage, which plots to the left of the simply saturated sample's curve is reached faster, with a more clearly defined yield point, indicating that the strength of the original intact structure has been "weakened" during the flow.

The data for the undisturbed specimens, which are not fully saturated and were tested under constant-water content conditions, are plotted in terms of total stress. In unsaturated soils, the location of the compression curve in a plot of specific volume vs. total stress depends on the specimen's suction. Compression tests carried out while controlling the suction to remain constant follow a curve representing that suction value, and for any given soil there is a family of compression curves corresponding to different values of suction. In compression tests carried out under constant-water conditions, as is the case here, the suction is not constant and decreases with increasing confining stress. The apparent slope of the curves obtained for the undisturbed specimens, which is steeper than that obtained in saturated conditions, corresponds therefore to the compression curve crossing contours of decreasing suction as the confining stress increases.

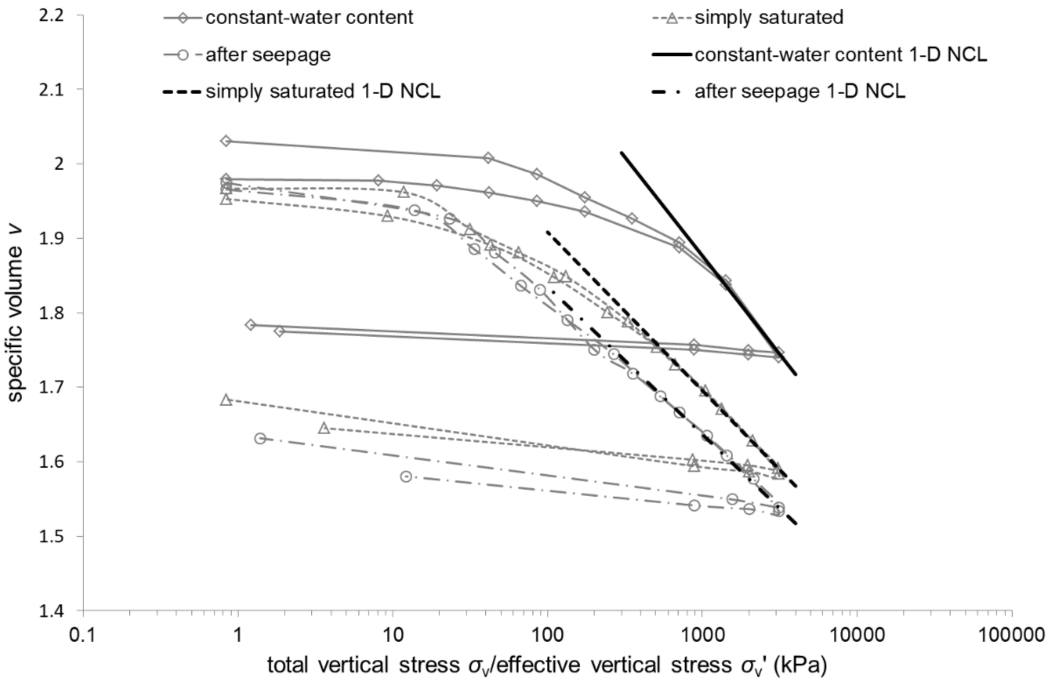

5(a)

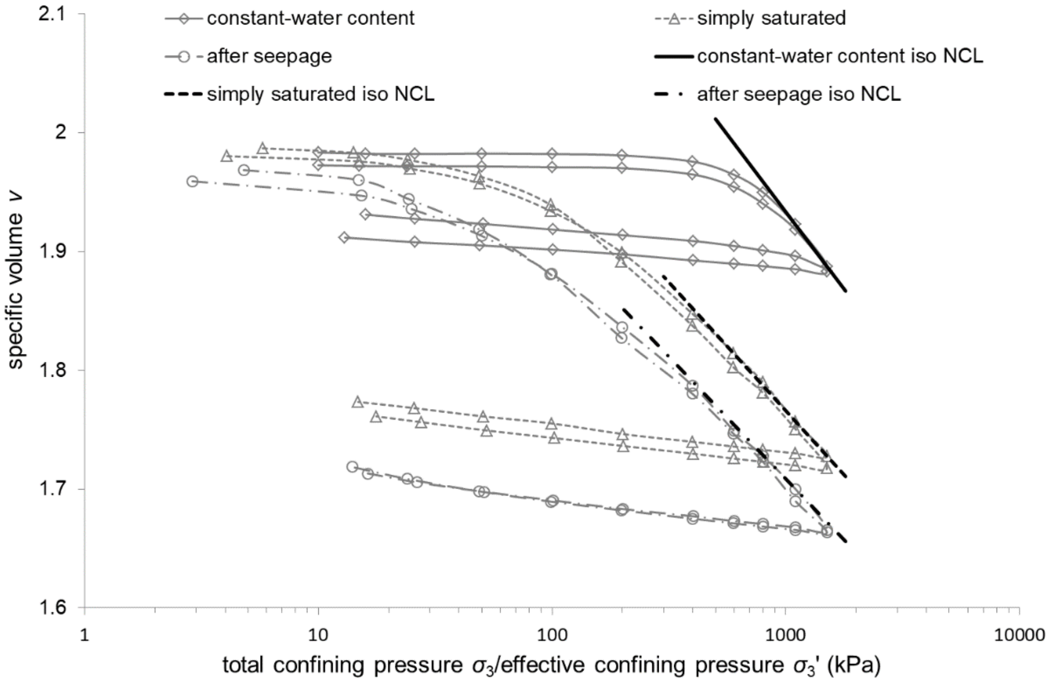

5(b)

Figure 5 Compression curves with normal compression lines (NCLs) of undisturbed specimens in different water conditions (a) one-dimensional compression (b) isotropic compression

The isotropic and one-dimensional compression curves (Intrinsic Compression Lines (ICL) for the isotropic curves) of reconstituted silty loess specimens are shown in figure 6. Again the data for the tests performed at natural water content are shown in terms of total stress, while the data for the saturated tests are shown in term on effective stress. The triaxial specimens with relatively high initial specific volume that underwent saturation and seepage processes experienced an initial collapse, monitored by the local LVDTs (figure 6b), which was not found with the undisturbed specimens, probably due to the existence of an intact, more stable structure. Another difference is the lack of complete convergence between the compression curves of a given water condition. For the specimens with relatively low initial specific volume, this could be because much higher stress levels are needed to induce large enough volumetric strains to reach the NCL (Li & Coop, 2019). An overall downward shift can still be observed as the sample undergoes a steady flow of water, while the difference between ICLs under simply saturation and after seepage becomes less significant compared to the NCLs of the undisturbed specimens.

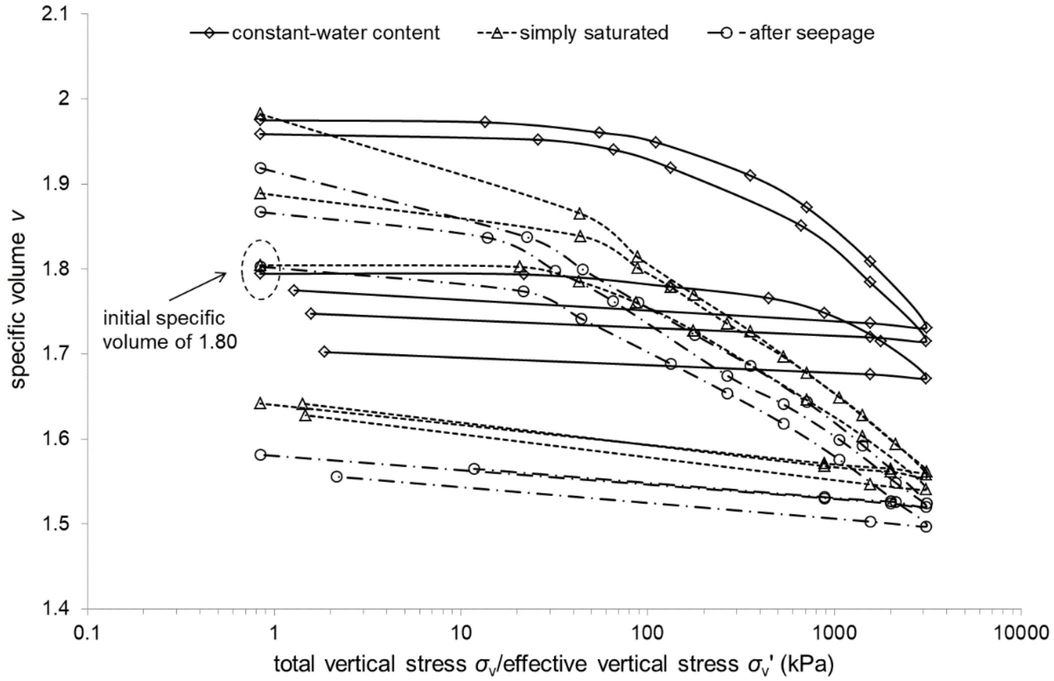

6(a)

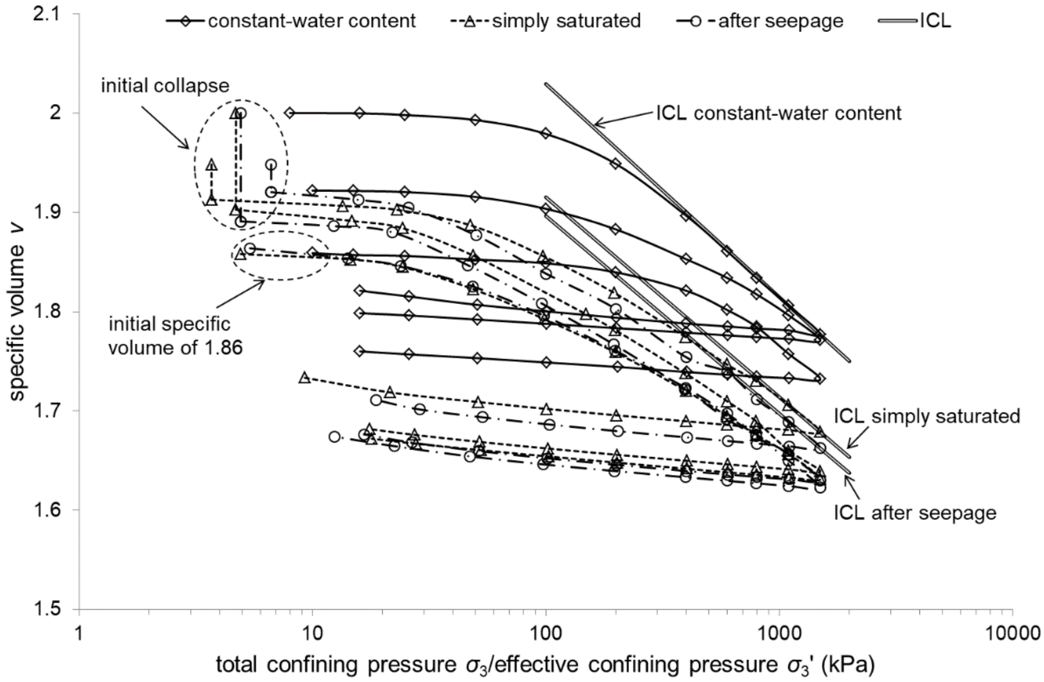

6(b)

Figure 6 Compression curves of reconstituted specimens in different water conditions (a) one-dimensional compression (b) isotropic compression with intrinsic compression lines (ICLs)

Small strain behaviour

~~Bender element tests were carried out during the isotropic compression tests.~~

G_0 under different water conditions

The small strain stiffness G_0 of specimens was measured at the confining pressure of 50kPa (total for unsaturated and effective for saturated). In figure 7a, a comparison between the stiffnesses of undisturbed and reconstituted specimens under constant-water content and simply saturated conditions shows that both the remolding and the saturation affect the stiffness G_0, with decreased values from 1/6 to 1/3 of the undisturbed soil stiffness. For these samples, the stiffness remains constant over a period of 24hrs, as has been reported by others (e.g. Song et al., 2017).

The effect of seepage on the small strain stiffness is shown in figure 7b where G_0 was measured at an effective pressure of 50kPa at different times and therefore outflow water volumes, until the coefficient of permeability became stable. The seepage was temporarily stopped and the back pressure was kept at 0kPa when the measurement was conducted, to ensure an exact effective stress of 50kPa. In both the undisturbed and reconstituted specimens, the value of G_0 decreases continuously until becoming constant at an outflow volume of 900ml, which is about 5 times the specimen volume. This decrease in G_0, under the same confining pressure, indicates a degradation of soil structure as water flows through the sample, more pronounced in the undisturbed specimen.

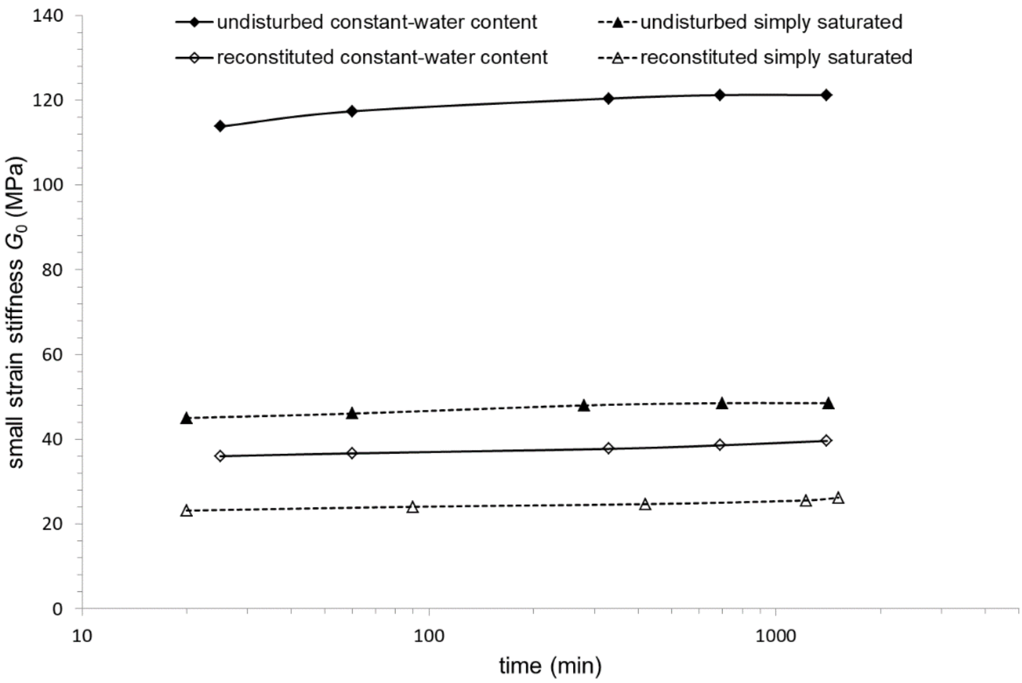

7(a)

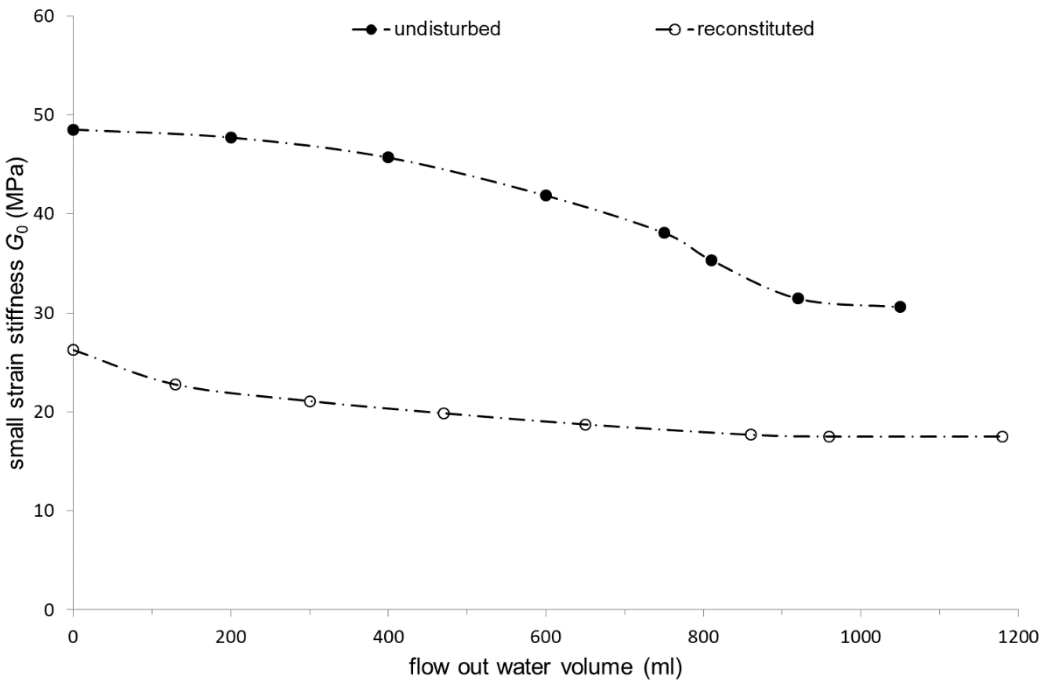

7(b)

Figure 7 Small strain stiffness of specimens in different water conditions at isotropic stress state of 50kPa (a) constant-water content and simply saturated conditions (b) after seepage condition

G_0 under different confining stresses

The relationship between small strain stiffness and effective stress is investigated in figure 8 where bender element test data are plotted for both the undisturbed and reconstituted specimens, under different saturated flow conditions. A unique line is identified after yielding for each type of saturated test, indicating the existence of distinct normal compression lines in terms of $\ln G_0$-$\ln\sigma_3'$. Two parallel lines can be determined for the undisturbed samples under saturated conditions, the specimen after steady flow plotting lower than the simply saturated one. The constant-water content sample is plotted in terms of total stress, with a much higher stiffness. The data for the reconstituted specimens, both simply saturated and after seepage flow, plot on a single line, almost parallel but lower than those for the undisturbed samples.

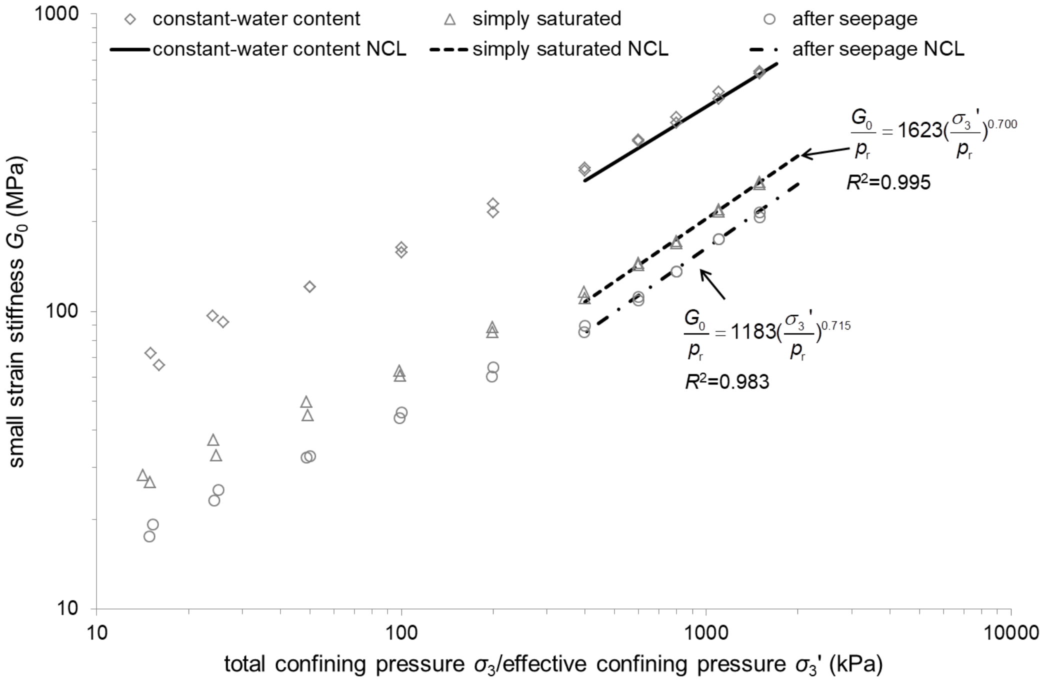

8(a)

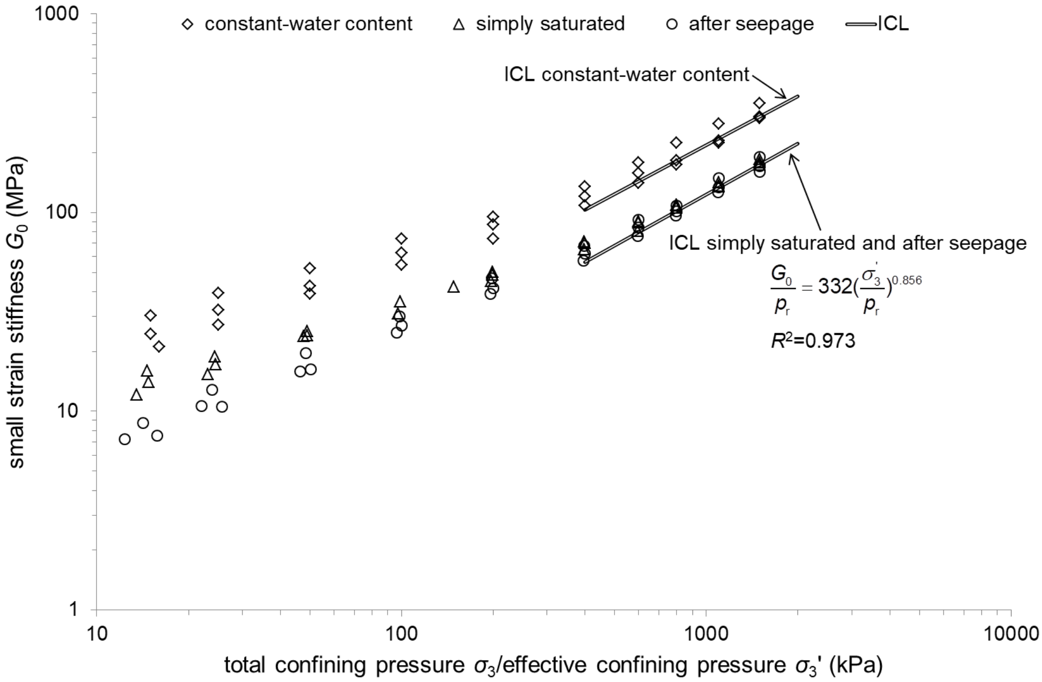

8(b)

Figure 8 Small strain stiffness of specimens in different water conditions under isotropic compression (a) undisturbed (b) reconstituted

The mechanism of seepage water induced degradation

The mechanism of seepage-induced structure degradation was investigated by means of microscopic and chemical analyses. The coefficient of permeability, k, of the undisturbed and reconstituted specimen subjected to seepage conditions under a constant isotropic effective confining pressure of 50kPa was calculated during the seepage process by:

$$k = \frac{qL}{60Sh} \tag{10}$$

where q is the volume of water outflow per minute, L is the length of specimen, S is the area of the cross section of specimen, and h is the seepage water head (which is 1m in this study). The coefficient was determined at different cumulative volumes of water outflow. Figure 9 shows that despite the initial difference due to a more disturbed structure of the reconstituted specimen (similar void ratio but fewer macropores), the coefficient for both samples decreases during seepage and reaches the same constant value. It has been reported that for compacted clays or clayey soils, the hydraulic conductivity is significantly influenced by the size of the aggregate and the percentage of fine particles (Benson & Daniel, 1990; Kenney et al., 1992; Benson & Trast, 1995), larger aggregate sizes and fewer fine particles can provide larger voids in between, and thus higher permeability. It then can be inferred that for both the undisturbed and reconstituted silty loess, there is possible disintegration of soil aggregates during seepage, resulting in smaller aggregate size and more fine particles, and thus lower permeability.

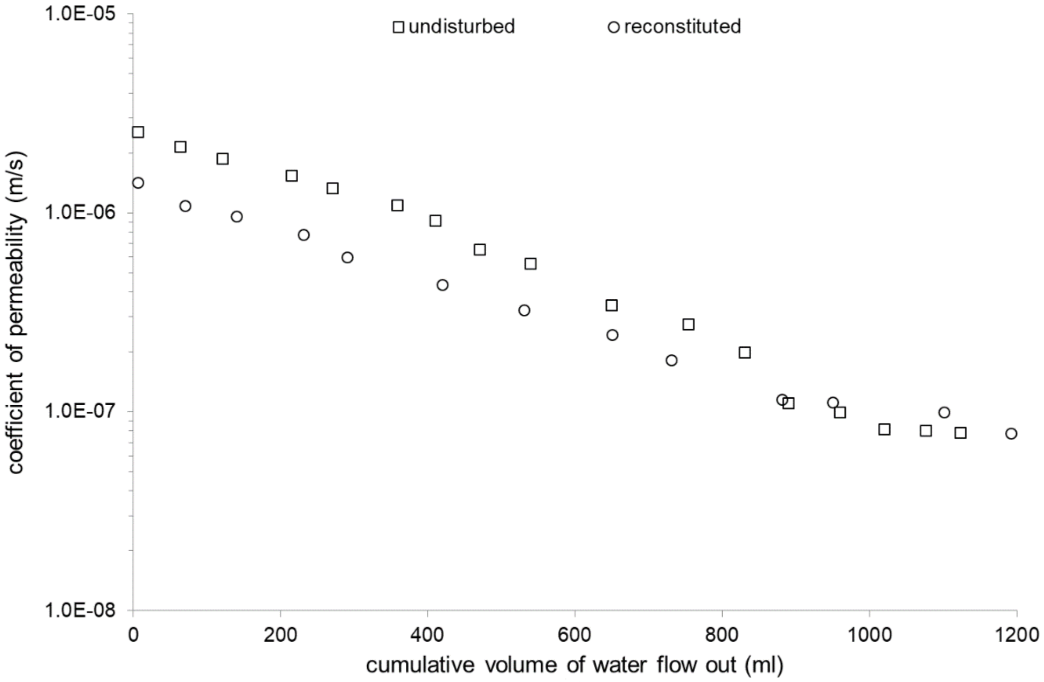

Figure 9 Variation of permeability coefficient of undisturbed and reconstituted specimens during seepage

After seepage, samples were also collected from different points of the undisturbed specimen for pore size distribution (by mercury intrusion porosimetry (MIP)) and grain size distribution, together with the intact original sample. The MIP test results in figure 10a show that before seepage, the pore size distribution of intact sample has a major peak around 15μm, and no obvious minor peaks can be observed. After seepage, the major pore sizes reduce to less than 7μm for all sample points, and some minor peaks can be found between 0.1 and 1μm. The decrease in pore size explains the decrease in coefficient of permeability after seepage. It has been reported that dry-side compacted clays and clayey silts generally have a bimodal pore size distribution

(Delage et al., 1996; Romero, 2013), when subject to water infiltration, the aggregates in soil will expand and occupy the macropores in between, resulting in the decrease in macropore size and increase in micropore size, and thus a less bimodal distribution shape and a lower permeability (Alonso et al., 2011; Romero et al., 2011; Musso et al., 2013). While the evolution of pore size of intact silty loess during seepage seems different, considering the low aggregates expanding potential due to the low clay content, the decrease in macropore size is more likely to be caused by the fine particles detached from the aggregates, and the increase in the amount of micropores can also be an evidence of the increase of free fine particles. Meanwhile, the results from the grain size distribution (figure 10b) show that there is no significant difference among different points in particle size before and after seepage, indicating no further suffusion occurred during the whole process. Then it can be concluded that particle rearrangement occurs locally during seepage, and the pore size between primary silt particles and aggregates is reduced.

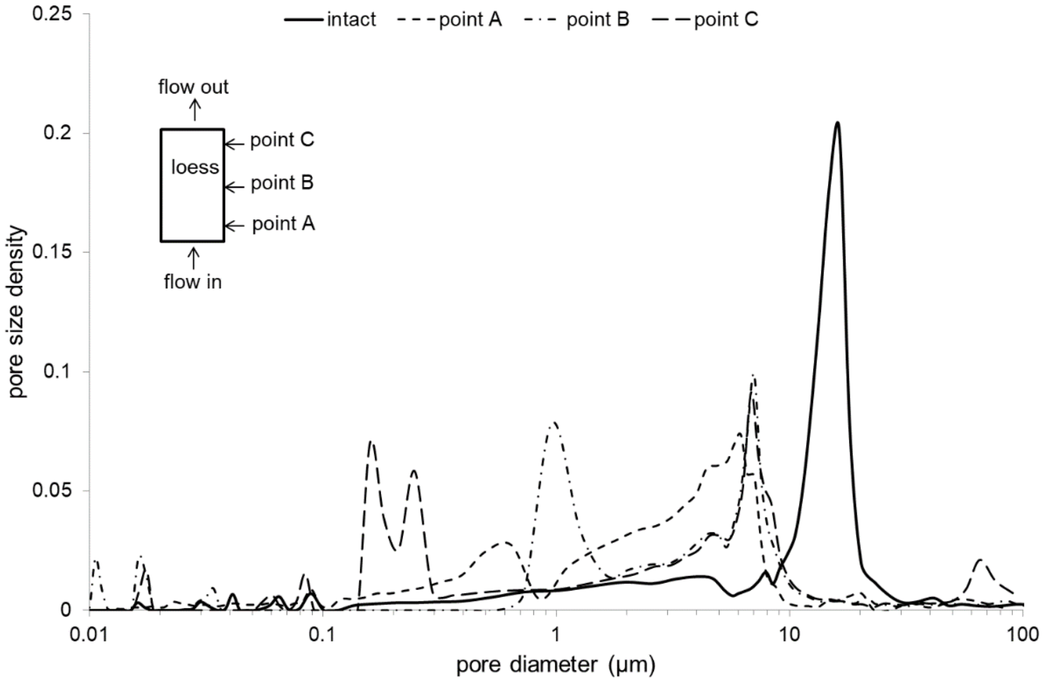

10(a)

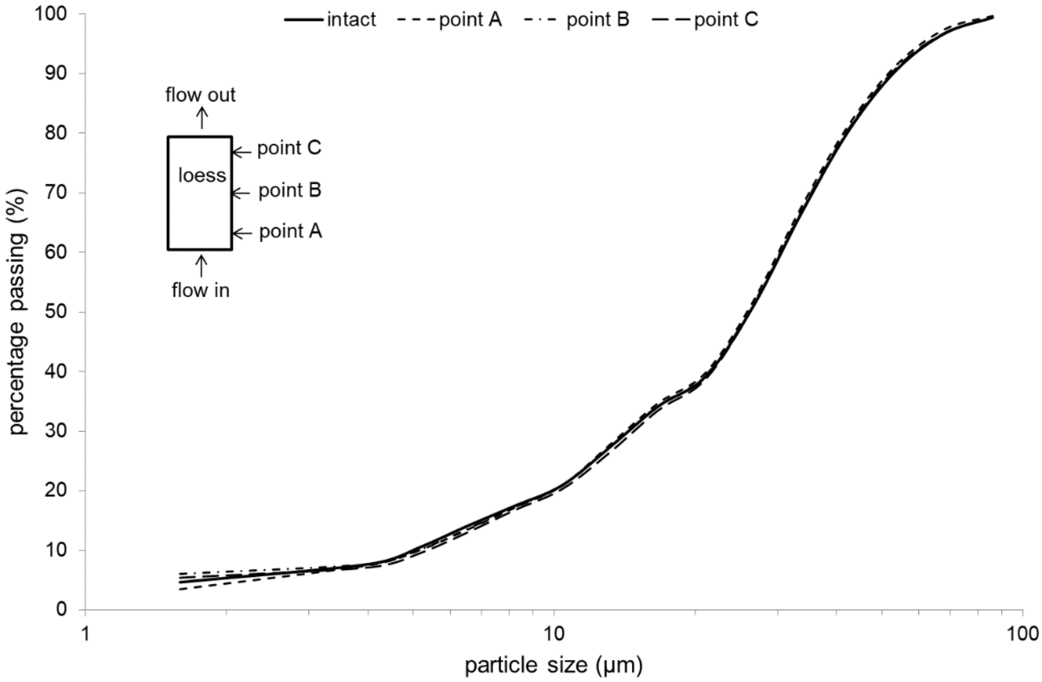

10(b)

Figure 10 MIP test and PSD analysis results of undisturbed specimen before and after seepage (a) pore sizes density (b) cumulative particle size distribution

A scanning electron microscope (SEM) test was conducted with the undisturbed loess specimen before and after seepage to have a more direct look at the soil structure. The specimens were cut into small pieces with attention to the direction to ensure the cross section surface was tested, and the results are shown in figure 11. It shows in figure 11a that in undisturbed soil, secondary (small-sized) silt particles are more likely to be bonded with some primary silt particles to form aggregates, and the primary silt particles and aggregates are bonded at the contacts to form the soil structure, with apparent macropores in between. While after seepage, as shown in figure 11b, it seems that instead of bonding to primary silt particles, some secondary silt particles are more likely to exist separately and fill in the pore space between large particles or aggregates, which reduces the pore size. It indicates that the long term seepage may have an effect to first weaken the bonding within the soil structure, then create detached small silt particles, and further transport them into the pores.

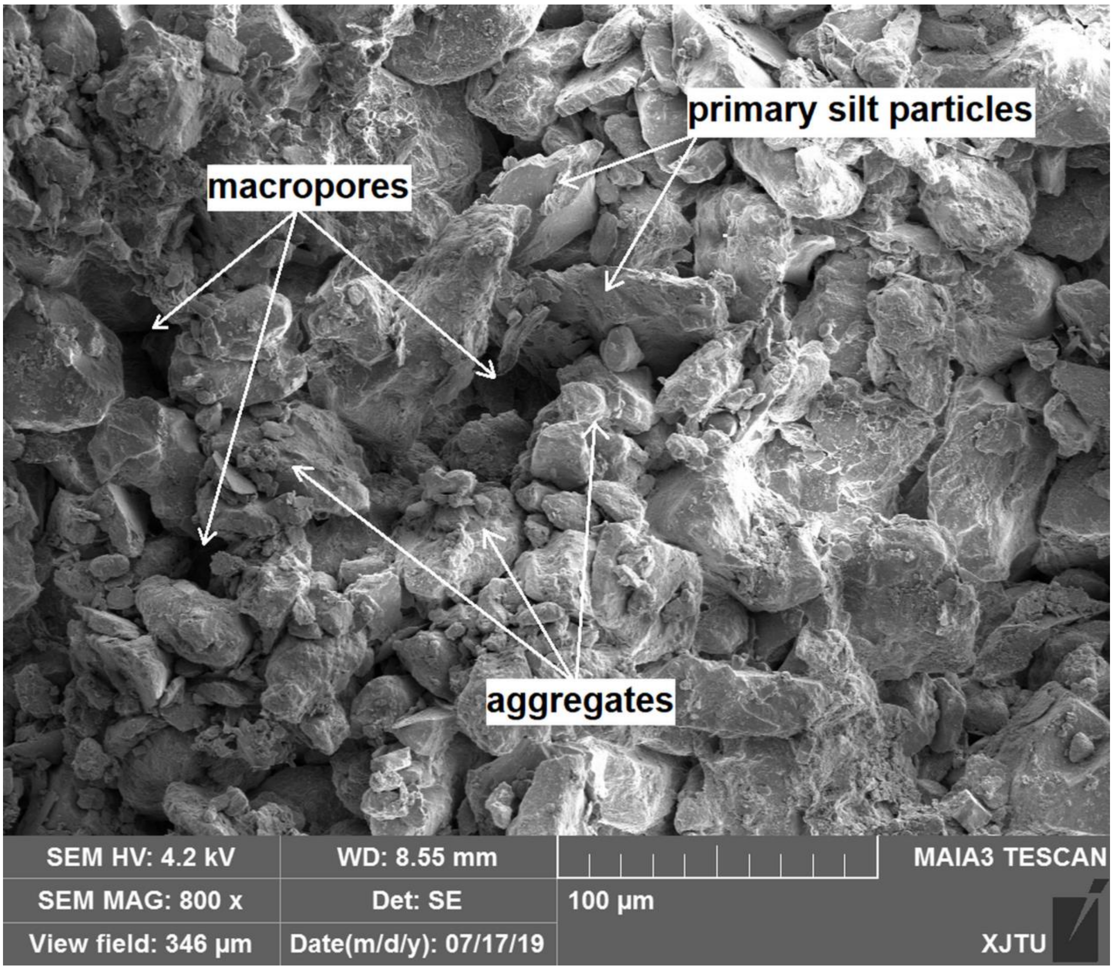
primary silt particles
macropores
aggregates
SEM HV: 4.2 kV
WD: 8.55 mm
MAIA3 TESCAN
SEM MAG: 800 x
Det: SE
100 μm
View field: 346 μm
Date(m/d/y): 07/17/19
XJTU

11(a)

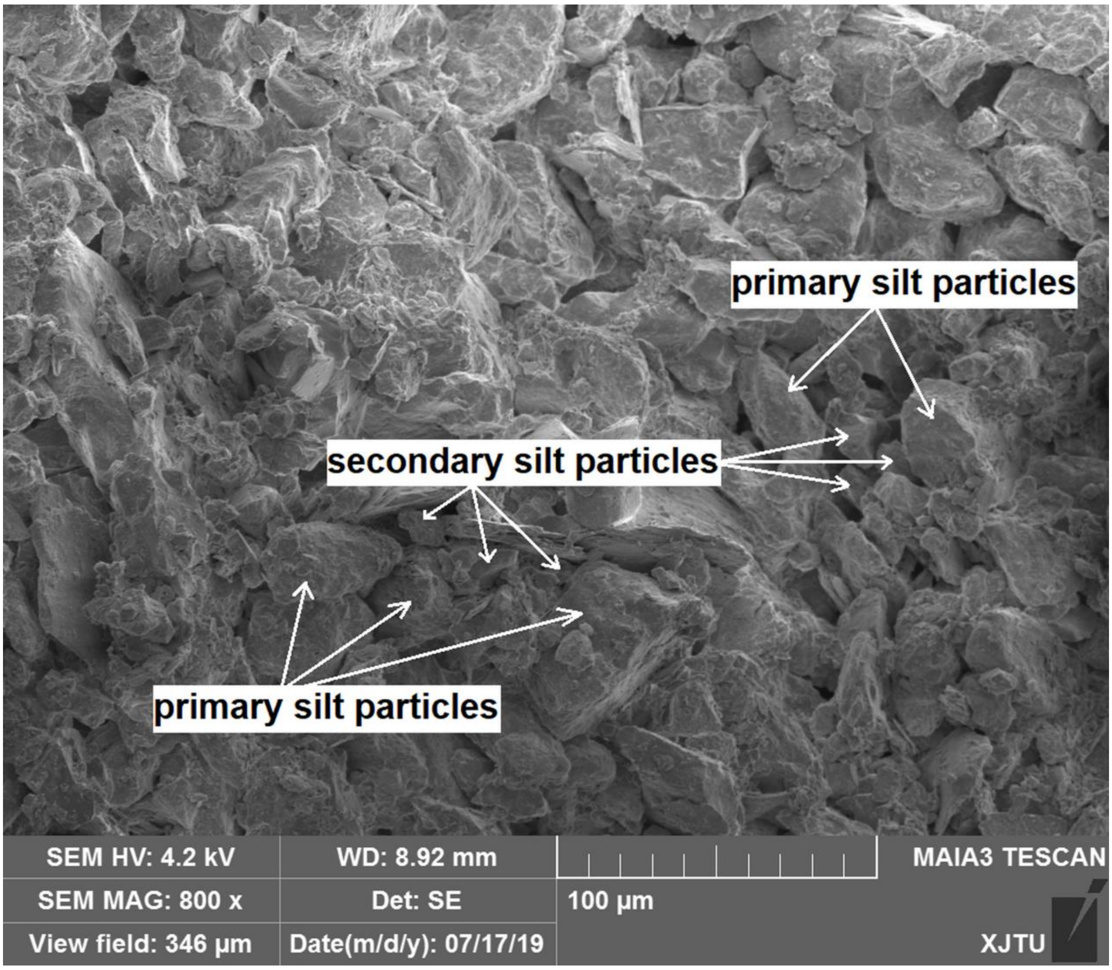

11(b)

Figure 11 SEM images of undisturbed specimen before and after seepage showing different soil structures (a) before (b) after

The bonding material of loess structure is reported mainly to be clay minerals and calcium carbonate (e.g. Li et al., 2016; Jiang et al., 2012). The calcium carbonate is relatively stable in pore water, while the mechanical properties of clays are reported to be related to the pore fluid composition, particularly for illite, the major clay mineral in loess, the decrease in pore ion concentration can cause strength loss (e.g. Zhang et al., 2013; Fan et al., 2017). Loess contains soluble salts with cation mainly as Na^+, and medium soluble salts with cation mainly as Ca^{2+} (e.g. Li et al., 2016). It is also reported that in natural condition, the soluble salts are already dissolved with high concentration (Fan et al., 2017). The outflow water of the undisturbed loess specimen was therefore collected at different cumulative volumes to test the Na^{+} and Ca^{2+} concentrations, and the results are plotted in figure 12. It shows that Na^{+} only exists at the start of the outflow, while Ca^{2+} can be observed during the whole seepage process. It indicates that by saturation, the structure degradation due to bonding strength loss can be caused by the significant decrease in the concentration of soluble salt cations; while during seepage, the degradation of soil structure and strength can develop further due to the initial loss of soluble salt cations and the continuous loss of medium soluble salt cations, which are caused by the seepage water leaching.

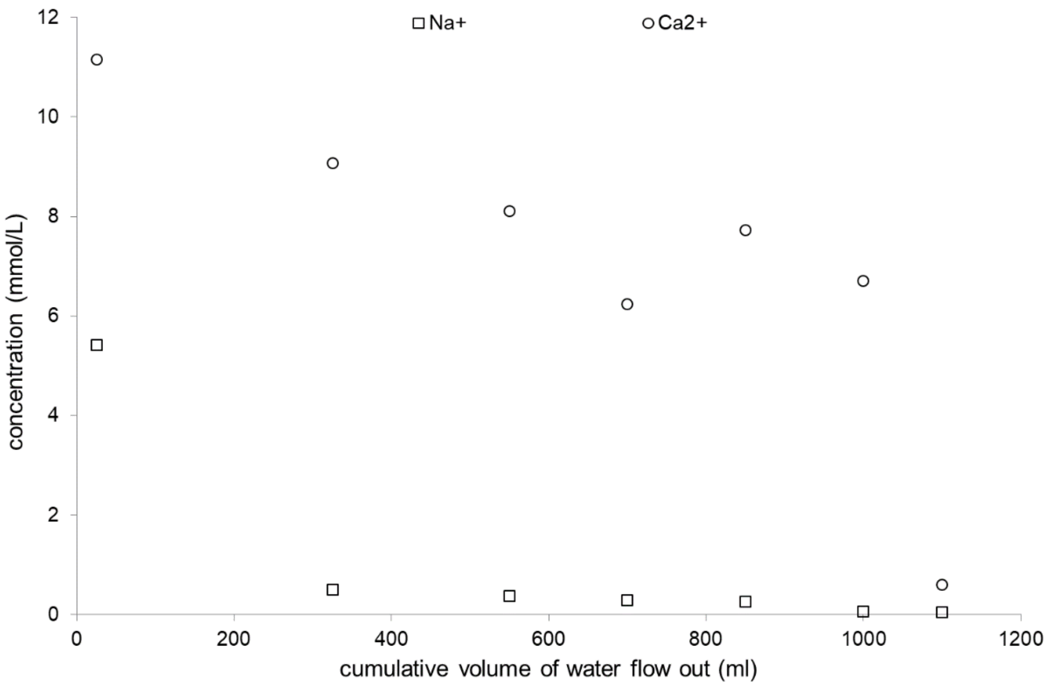

Figure 12 Variation of Na^{+} and Ca^{2+} concentrations in the outflow seepage water of

the undisturbed specimen

Conclusion

Both undisturbed and reconstituted specimens of a typical silty loess were tested to study the mechanical behaviour under different water conditions, especially in long-term seepage condition. Both the compression yield stress and the small strain stiffness were found to decrease during seepage, with a more significant reduction in the undisturbed samples. This was accompanied by a marked increase in compressibility post-yield, with all effects suggesting a significant degradation of structure during seepage.

It can be concluded from the compression results that the loess yields earlier at low stress levels and show larger compressibility after long-term steady state seepage. Similarly, a negative effect is found with the small strain stiffness data obtained during compression. As the specimen is subjected longer to seepage, the decrease in G_0 is observed, indicating a less stable soil structure.

With a closer investigation of the evolution of soil structure formation and pore ions concentration during seepage, it is postulated that as the soluble and medium soluble salts in loess are leached out by seepage water, the pore ions concentration decreases and results in a loss of clay mineral bonding strength. Then some of the smaller-sized silt particles are more likely to be detached from the aggregates, and the soil structure is thus weakened. This highlights that the outflow in field at the slope edge should be monitored as salt deposits have already been observed on the loess surface in slope areas, and that may cause large deformations in the long-term.

Acknowledgement

The work was supported by the National Natural Science Foundation of China (Project No. 41772316), the Major Program of National Natural Science Foundation of China (Project No. 41790441), the National Key Research and Development Plan (Project No. 2018YFC1504701), the China Postdoctoral Science Foundation (Project No. 2019M663729) and the Key Research Platform Open Fund Project (Project No. 300102219520).

Notations

G_0 small strain stiffness

p' mean effective stress

p_r reference stress taken as 1kPa

A soil small strain stiffness parameter

n soil small strain stiffness parameter

σ_v total normal stress in one dimensional compression

σ_3 total confining stress in isotropic compression

σ_v' effective normal stress in one dimensional compression

σ_3' effective confining stress in isotropic compression

v specific volume

v_i initial specific volume

G_s specific gravity

γ_w unit weight of water

γ_{di} initial dry unit weight

γ_i initial bulk unit weight

γ_f final bulk unit weight

w_i initial water content

w_f final water content

ε_v volumetric strain

ε_a axial strain

ε_r radial strain

$\Delta\varepsilon_v$ volumetric strain increment

k coefficient of permeability

q volume of water flow out per minute

L length of specimen

S area of the cross section of specimen

h seepage water head

References

Ackerley, S.K., Standing, J.R., Hosseini Kamal, R. (2016). A system for measuring radial local strains in triaxial apparatus. *Géotechnique* **66**, No. 6, 515-522.

Alonso, E.E., Romero, E., Hoffmann C. (2011). Hydromechanical behaviour of compacted granular expansive mixtures: experimental and constitutive study. *Géotechnique* **61**, No. 4, 329-344.

Benson, C.H. & Daniel, D.E. (1990). Influence of clods on hydraulic conductivity of compacted clay. *Journal of Geotechnical Engineering* **116**, No. 8, 1231-1248.

Benson, C.H. & Trast, J.M. (1995). Hydraulic conductivity of thirteen compacted clay. *Clays and Clay Minerals* **43**, No. 6, 669-681.

Bjerrum, L. (1954). Geotechnical properties of Norwegian marine clays. *Géotechnique* **4**, No. 2, 49-69.

Bjerrum, L. & Rosenqvist, I.T. (1956). Some experiments with artificially sedimented clays. *Géotechnique* **6**, No. 3, 124-136.

Burland, J.B. (1990). On the compressibility and shear strength of natural clays. Thirties Rankine Lecture. *Géotechnique* **40**, No. 3, 329-378.

Cascante, G. & Santamarina, J.C. (1996). Interparticle contact behaviour and wave propagation. *Journal of Geotechnical Engineering* **122**, No. 10, 831-839.

Cho, G.C., Dodds, J.S., Santamarina, J.C. (2006). Particle shape effects on packing density, stiffness, and strength: natural and crushed sands. *Journal of Geotechnical and Geoenvironmental Engineering*, *ASCE* **132**, No. 5, 591-602.

Delage, P., Audiguier, M., Cui, Y., Howat, M.D. (1996). Microstructure of a compacted silt. *Canadian Geotechnical Journal* **33**, No. 1, 150-158.

Derbyshire, E., Dijkstra, T.A., Smalley, I.J., Li, Y.J. (1994). Failure mechanisms in loess and the effects of moisture content changes on remolded strength.

Quaternary International **24**, 5-15.

Di Maio, C. & Fenelli, G.B. (1994). Residual strength of kaolin and bentonite: the influence of their constituent pore fluid. *Géotechnique* **44**, No. 4, 217-226.

Di Maio, C. (1996). Exposure of bentonite to salt solution: osmotic and mechanical effects. *Géotechnique* **46**, No. 4, 695-707.

Di Maio, C., Scaringi, G., Vassallo, R. (2015). Residual strength and creep behaviour on the slip surface of specimens of a landslide in marine origin clay shales: influence of pore fluid composition. *Landslides* **12**, No. 4, 657-667.

Di Maio, C. & Scaringi, G. (2016). Shear displacement induced by decrease in pore solution concentration on a pre-existing slip surface. *Engineering Geology* **200**, 1-9.

Fan, X., Xu, Q., Scaringi, G., Li, S., Peng, D. (2017). A chemo-mechanical insight into the failure mechanism of frequently occurred in the Loess Plateau, Gansu Province, China. *Engineering Geology* **228**, 337-345.

Fannin, R.J. & Slangen, P. (2014). On the distinct phenomena of suffusion and suffosion. *Géotechnique Letters* **4**, No. 4, 289-294.

Heller, F. & Liu, T.S. (1982). Magnetostratigraphical dating of loess deposits in China. *Nature* **300**, 431-433.

Hunter, R.P. & Bowman, E.T. (2018). Visualisation of seepage-induced suffusion and suffusion within internally erodible granular media. *Géotechnique* **68**, No. 10, 918-930.

Jiang, M., Hu, H., Liu, F. (2012). Summary of collapsible behaviour of artificially structured loess in oedometer and triaxial wetting tests. *Canadian Geotechnical Journal* **49**, No. 10, 1147-1157.

Jiang, M., Zhang, F., Hu, H., Cui, Y., Peng, J. (2014). Structural characterization of natural loess and remolded loess under triaxial tests. *Engineering Geology* **181**, 249-260.

Jovičić, V. & Coop, M.R. (1997). Stiffness of coarse-grained soils at small strains. *Géotechnique* **47**, No. 3, 545-561.

Kenney, T.C., Van Veen, W.A., Swallow, M.A., Sungaila, M.A. (1992). Hydraulic conductivity of compacted bentonite-sand mixtures. *Canadian Geotechnical Journal* **29**, No. 3, 364-347.

Lee, J.S., Dodds, J., Santamarina, J.C. (2007). Behaviour of rigid-soft particle mixtures. *Journal of Materials in Civil Engineering*, *ASCE* **19**, No. 2, 179-184.

Leng, Y., Peng, J., Wang, Q., Meng, Z., Huang, W. (2018). A fluidized landslide occurred in the loess plateau: a study on loess landslide in south Jingyang tableland. *Engineering Geology* **236**, 129-136.

Li, C., Qi, J., Wang, S., Yang, L., Yang, W., Zou, S., Zhu, G., Li, W. (2014). A holistic approach to understanding underground water dynamics in the loess tableland: a case study of the Dongzhi loess tableland in Northwest China. *Water Resources Management* **28**, 2937-2951.

Li, P., Vanapalli, S.K., Li, T. (2016). Review of collapse triggering mechanism of collapsible soils due to wetting. *Journal of Rock Mechanics and Geotechnical Engineering* **8**, No. 2, 256-274.

Li, W. & Coop, M.R. (2019). Mechanical behaviour of Panzhihua iron tailings. *Canadian Geotechnical Journal* **56**, No. 3, 420-435.

Liu, F., Xu, Q., Zhang, Y., Frost, J.D., Zhang, X. (2019). State-dependent flow instability of a silty loess. *Géotechnique Letters* **9**, No. 1, 22-27.

Liu, X., Zhang, N., Lan, H. (2019). Effects of sand and water contents on the small-strain shear modulus of loess. *Engineering Geology* **260**, 105202.

Muñoz-Castelblanco, J., Delage, P., Pereira, J.M., Cui, Y.J. (2011). Some aspects of the compression and collapse behaviour of an unsaturated natural loess. *Géotechnique Letters* **1**, No. 2, 17-22.

Musso, G., Romero, E., Della Vecchia, G. (2013). Double-structure effects on the chemo-hydro-mechanical behaviour of a compacted active clay. *Géotechnique* **63**, No. 3, 206-220.

Ng, C.W.W., Mu, Q.Y., Zhou, C. (2017a). Effects of soil structure on the shear behaviour of an unsaturated loess at different suctions and temperatures. *Canadian Geotechnical Journal* **54**, No. 2, 270-279.

Ng, C.W.W., Kaewsong, R., Zhou, C., Alonso, E.E. (2017b). Small strain shear moduli of unsaturated natural and compacted loess. *Géotechnique* **67**, No. 7, 646-651.

Rocchi, I. & Coop, M. R. (2014). Experimental accuracy of the initial specific volume. *Geotechnical Testing Journal* **37**, No. 1, 169–175.

Rogers, C.D.F., Dijkstra, T.A., Smalley, I.J. (1994). Hydroconsolidation and subsidence of loess: Studies from China, Russia, North America and Europe: In memory of Jan Sajgalik. *Engineering Geology* **37**, No. 2, 83-113.

Romero, E. (2013). A microstructural insight into compacted clayey soils and their hydraulic properties. *Engineering Geology* **165**, 3-19.

Romero, E., Della Vecchia, G., Jommi, C. (2011). An insight into the water retention properties of compacted clayey soils. *Géotechnique* **61**, No. 4, 313-328.

Song, B., Tsinaris, A., Anastasiadis, A., Pitilakis, K., Chen, W. (2017). Small-strain stiffness and damping of Lanzhou loess. *Soil dynamics and Earthquake Engineering* **95**, 96-105.

Tang, Y.M., Xue, Q., Li, Z.G., Feng, W. (2015). Three modes of rainfall infiltration inducing loess landslide. *Natural Hazards* **79**, No. 1, 137-150.

Tiwari, B., Tuladhar, G.R., Marui, H. (2005). Variation in residual shear strength of the soil with the salinity of pore fluid. *Journal of Geotechnical and Geoenvironmental Engineering*, *ASCE* **131**, No. 12, 1445-1456.

Tiwari, B. & Ajmera, B. (2015). Reduction in fully softened shear strength of natural clays with NaCl leaching and its effect on slope stability. *Journal of Geotechnical and Geoenvironmental Engineering*, *ASCE* **141**, 04014086.

Tu, X.B., Kwong, A.K.L., Dai, F.C., Tham, L.G., Min, H. (2009). Field monitoring of rainfall infiltration in a loess slope and analysis of failure mechanism of rainfall-induced landslides. *Engineering Geology* **105**, 135-150.

Viggiani, G. & Atkinson, J.H. (1995). Stiffness of fine-grained soil at very small strains. *Géotechnique* **45**, No. 2, 249-265.

Wang, W., Wang, Y., Sun, Q., Zhang, M., Qiang, Y., Liu, M. (2018). Spatial variation of saturated hydraulic conductivity of a loess slope in the South Jingyang Plateau, China. *Engineering Geology* **236**, 70-78.

Wen, B.P. & Yan, Y.J. (2013). Influence of structure on shear characteristics of the unsaturated loess in Lanzhou, China. *Engineering Geology* **168**, 46-58.

Xie, W., Li, P., Vanapalli, S.K., Wang, J. (2018). Prediction of the wetting-induced collapse behaviour using the soil-water characteristic curve. *Journal of Asian Earth Sciences* **151**, 259-268.

Xu, L., Dai, F.C., Tham, L.G., Tu, X.B., Min, H., Zhou, Y.F., Wu, C.X., Xu, K. (2011). Field testing of irrigation effects on the stability of a cliff edge in loess, North-west China. *Engineering Geology* **120**, 10-17.

Xu, L., Dai, F.C., Gong, Q.M., Tham, L.G., Min, H. (2012). Irrigation-induced loess flow failure in Heifangtai platform, North-West China. *Environmental Earth Sciences* **66**, No. 6, 1707-1713.

Xu, L., Dai, F., Tu, X., Tham, L.G., Zhou, Y., Iqbal, J. (2014). Landslides in a loess platform, North-west China. *Landslides* **11**, No. 6, 993-1005.

Xu, L. & Coop, M.R. (2016). Influence of structure on the behaviour of a saturated clayey loess. *Canadian Geotechnical Journal* **53**, No. 6, 1026-1037.

Xu, L. & Coop, M.R. (2017). The mechanics of a saturated silty loess with a transitional mode. *Géotechnique* **67**, No. 7, 581-596.

Xu, L., Coop, M.R., Zhang, M.S., Wang, G.L. (2018). The mechanics of a saturated silty loess and implications for landslides. *Engineering Geology* **236**, 29-42.

Zeng, R.Q., Meng, X.M., Zhang, F.Y., Wang, S.Y., Cui, Z.J., Zhang, M.S., Zhang, Y., Chen, G. (2016). Characterizing hydrological processes on loess slopes using electrical resistivity tomography – a case study of the Heifangtai terrace, Northwest China. *Journal of Hydrology* **541**, 742-753.

Zhang, D.X., Wang, G.H., Luo, C., Chen, J., Zhou, Y. (2009). A rapid loess flowslide triggered by irrigation in China. *Landslides* **6**, No. 1, 55-60.

Zhang, F., Wang, G., Kamai, T., Chen, W., Zhang, D., Yang, J. (2013). Undrained shear behavior of loess saturated with different concentrations of sodium chloride solution. *Engineering Geology* **155**, 69-79.

Zhang, F., Kang, C., Chan, D., Zhang, X., Pei, X., Peng, J. (2017). A study of a flowslide with significant entrainment in loess areas in China. *Earth Surface Processes and Landforms* **42**, No. 14, 2295-2305.

Zhang, F. & Wang, G. (2018). Effect of irrigation-induced densification on the post-failure behavior of loess flowslides occurring on the Heifangtai area, Gansu, China. *Engineering Geology* **236**, 111-118.

Zhao, C., Shao, M., Jia, X., Nasir, M., Zhang, C. (2016). Using pedotransfer function to estimate soil hydraulic conductivity in the Loess Plateau of China. *Catena* **143**, 1-6.

Zhou, Y.F., Tham, L.G., Yan, W.M., Dai, F.C., Xu, L. (2014). Laboratory study on soil behavior in loess slope subjected to infiltration. *Engineering Geology* **183**, 31-38.

List of tables and figures

Table 1 Mineral composition of the silty loess

Table 2 Summary of tests conducted with the silty loess

Figure 1 The leaching out of salt induced by water seepage in field

Figure 2 Particle size distribution curve of silty loess

Figure 3 Schematic diagram triaxial apparatus equipped with vertical bender elements and axial and radial LVDTs

Figure 4 Ratios of the volumetric strain increments determined by two methods at different loading stages

Figure 5 Compression curves with normal compression lines (NCLs) of undisturbed specimens in different water conditions (a) one-dimensional compression (b) isotropic compression

Figure 6 Compression curves of reconstituted specimens in different water conditions (a) one-dimensional compression (b) isotropic compression with intrinsic compression lines (ICLs)

Figure 7 Small strain stiffness of specimens in different water conditions at isotropic 50kPa (a) constant-water content and simply saturated conditions (b) after seepage condition

Figure 8 Small strain stiffness of specimens in different water conditions under isotropic compression (a) undisturbed (b) reconstituted

Figure 9 Variation of permeability coefficient of undisturbed and reconstituted specimens during seepage

Figure 10 MIP test and PSD analysis results of undisturbed specimen before and after seepage (a) pore sizes density distribution (b) cumulative particle size distribution

Figure 11 SEM images of undisturbed specimen before and after seepage showing different soil structures (a) before (b) after

Figure 12 Variation of Na^{+} and Ca^{2+} concentrations in the outflow seepage water of the undisturbed specimen